



Dalton
Transactions

**Azo-triazolide Bis-cyclometalated Ir(III) Complexes via
Cyclization of 3-Cyanodiarylformazanate Ligands**

| | |
|-------------------------------|-----------------------------------------------------------------------------------------------------------------------------------------------------------------------------------------------------------------------------------------------------------|
| Journal: | <i>Dalton Transactions</i> |
| Manuscript ID | DT-ART-10-2019-003914.R1 |
| Article Type: | Paper |
| Date Submitted by the Author: | 16-Nov-2019 |
| Complete List of Authors: | Mu, Ge ; University of Houston, Department of Chemistry Wen, Zhili; University of Houston, Department of Chemistry Wu, Judy I-Chia; University of Houston, Department of Chemistry Teets, Thomas; University of Houston, Department of Chemistry |
| | |

SCHOLARONE™
Manuscripts

ARTICLE

Azo-triazolide Bis-cyclometalated Ir(III) Complexes via Cyclization of 3-Cyanodiarylformazanate Ligands

Ge Mu, Zhili Wen, Judy I-Chia Wu, and Thomas S. Teets*

Received 00th January 20xx,
Accepted 00th January 20xx

DOI: 10.1039/x0xx00000x

In this work we describe the synthesis of sterically encumbered 1,5-diaryl-3-cyanoformazanate bis-cyclometalated iridium(III) complexes, two of which undergo redox-neutral cyclization during the reaction to produce carbon-bound 2-aryl-4-arylo-2H-1,2,3-triazolide ligands. This transformation offers a method for accessing 2-aryl-4-arylo-2H-1,2,3-triazolide ligands, a heretofore unreported class of chelating ligands. One formazanate complex and both triazolide complexes are structurally characterized by single-crystal X-ray diffraction, with infrared spectroscopy being the primary bulk technique to distinguish the formazanate and triazolide structures. All complexes are further characterized by UV-Vis absorption spectroscopy and cyclic voltammetry, with the triazolide compounds having similar frontier orbital energies to the formazanate complexes but much less visible absorption.

Introduction

1,2,3-triazoles, a class of five-membered heterocyclic aromatic molecules containing three consecutive nitrogen atoms, have attracted considerable attention over the past few decades, and continue to be developed further today.^{1–3} The synthetic chemistry of these organic molecules has been explored in considerable detail, with the well-known copper-catalyzed azide-alkyne Huisgen cycloaddition,⁴ the most popular of all “click” reactions, being the most widespread and enabling method for the construction of 1,2,3-triazole substructures. These compounds have been applied in energetic materials^{3,5–7} and also work as the core structures in a large variety of compounds with pharmaceutical applications,^{8–12} because of their high resistance to metabolic degradation and ability to hydrogen bond with biomolecules.

The ease of synthesis of a wide range of 1,2,3-triazole-based compounds, as well as the ability to include a variety of functional groups into the triazole core^{13–17} have led to a rich metal coordination chemistry for triazoles.^{18–21} The nitrogen-rich heterocycle can coordinate to metals in a variety of ways, and chelating ligands can be accessed by appending another donor group as a substituent. Deprotonation or C–H activation at the 5-position may allow access to anionic triazolides,^{22,23} while alkylation at the N–3 position, followed by deprotonation of the relatively acidic C–H bond, leads to the formation of abnormal mesoionic carbenes.^{24–26} As representative examples of 1,2,3-triazolide metal complexes, Straub and co-workers

have isolated a copper triazolide complex which has been crystallographically characterized,²⁷ Swager’s group has reported a method for the one-pot synthesis of tris-cyclometalated iridium triazolide complexes,²⁸ and Gray’s group has reported extensively on gold triazolides formed under similar conditions as the typical Huisgen cycloaddition route.^{29–31}

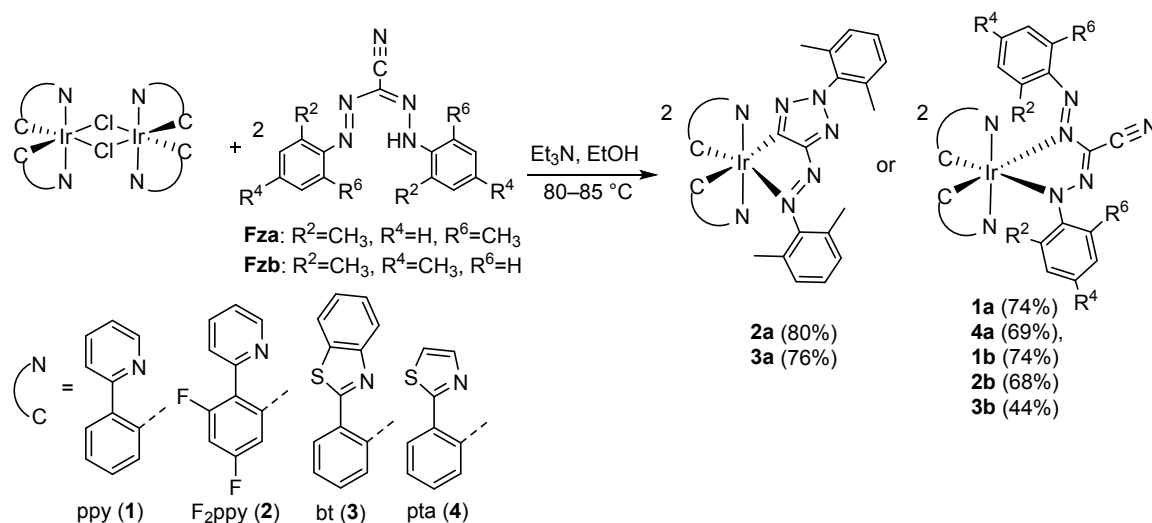
Despite the rich organic and coordination chemistry of 1,2,3-triazoles summarized above, some challenges remain in further diversifying this class of ligands. Nitrogen substituents in most click-derived 1,2,3-triazole ligands are limited to the N1 or N3 position,^{13,24,32–34} and while there are successful synthetic routes for preparing 2-substituted 1,2,3-triazoles,^{10,16,35–38} these structures remain rare in coordination compounds.^{10,39} In addition, although arylazo moieties are ubiquitous in many chelating redox-active ligands,⁴⁰ the azo-triazole ligand class has not been disclosed, presumably due to the incompatibility of copper-catalyzed Huisgen cycloadditions with azo functionalities and the observation that the few known azo-substituted triazoles are energetic materials.^{3,5,32}

These observations motivate continued pursuit of alternative methods for preparing N2-substituted azo-1,2,3-triazole complexes, to access chelating ligands that are not available by the typical click chemistry routes. Such an effort would require investigating alternative precursors for these ligands and exploring new reaction conditions that could allow their formation on a wider range of platforms. In this work, we show that carbon-bound 2-aryl-4-arylo-2H-1,2,3-triazolide bis-cyclometalated Ir(III) complexes, likely not accessible using Cu(I)-catalyzed cycloaddition reactions, can instead be prepared from 1,5-diaryl-3-cyanoformazan precursors. Formazanates, the monoanionic form of formazans, feature a 1,2,4,5-tetrazapentadiene (NNC₂NN) backbone, and the two additional nitrogen atoms greatly expand the redox chemistry of formazanates relative to the structurally related β-

University of Houston, Department of Chemistry, 3585 Cullen Blvd. Room 112, Houston, TX USA 77204-5003 Email: tteets@uh.edu

Electronic Supplementary Information (ESI) available: X-ray crystallographic tables, NMR spectra, IR spectra data, solvent-dependent absorption spectra, additional cyclic voltammograms, and optimized Cartesian coordinates from DFT calculations. CCDC 1946976–1946978. For ESI and crystallographic data in CIF or other electronic format see DOI: 10.1039/x0xx00000x

Scheme 1. General synthesis of complexes 1a–4a, 1b–3b.



diketiminates. The coordination chemistry of formazanates with many main group metals^{41–47} and first- and second-row transition metals^{48–52} has been established, and we have expanded the coordination chemistry of formazanates to third-row transition metals with a series of heteroleptic cyclometalated platinum complexes and bis-cyclometalated iridium complexes.^{53–55}

Well known for their multi-electron redox chemistry, recent work has also characterized the chemical reactivity of formazans, where reduction of formazanate complexes is sometimes accompanied by structural rearrangements. Examples include rearrangement of reduced boron formazanates to BN heterocycles,⁴⁶ electrophilic functionalization of reduced formazanate cores,⁵⁶ and our report that homoleptic platinum azo-iminate complexes can form via hydrogenative cleavage of formazans.⁵⁷ Otten's group also reported that arylazindazoles can be obtained via cyclization of C₆F₅-substituted formazans,⁵⁸ further highlighting the reactivity of formazans. The new mode of reactivity described here, which involves templated cyclization of 1,5-diaryl-3-cyanoformazans to form 2-aryl-4-arylazo-2H-1,2,3-triazolide chelates, is a redox-neutral cyclization that expands the chemical reactivity of formazanates and gives access to a new class of compounds. This reaction is not general for all diarylformazanates and in most cases the products remain as cyclometalated Ir(III) formazanate complexes, with the formazanate binding in the five-membered chelate "open" form we recently reported, involving coordination of N1 and N4 of the 1,2,4,5-tetraazapentadienyl core to the metal.⁵⁵ However, steric bulk on both the cyclometalating (C[^]N) ligands and the N-aryl substituents of formazanates appear to favor rearrangement to the triazolide form. In total we describe two triazolide complexes and five related formazanate complexes in this study. Three compounds (two triazolides and one formazanate) are structurally characterized by single-crystal X-ray diffraction, with infrared spectroscopy providing the most definitive evidence to distinguish the formazanate and

triazolide forms. Cyclic voltammetry and UV-Vis absorption spectroscopy are reported for all complexes, which demonstrate ligand-based redox chemistry and strong visible absorption for both classes of complexes. These electronic structural features are confirmed and further elaborated by DFT calculations on both formazanate and triazolide isomeric forms.

Results and discussion

Synthesis

Scheme 1 depicts the reaction conditions used to prepare the compounds described in this work. Compounds are numbered based on the identity of the cyclometalating ligand, with letters representing the two different formazan structures. Our previous work on cyclometalated iridium formazanate complexes⁵⁵ revealed two formazanate binding modes on these complexes, one the more typical six-member chelate involving the 1- and 5-positions of the formazan core, the other a five-member chelate involving the 1- and 4-positions. In an effort to further understand the structural preferences for these two different coordination modes, we began investigating the more sterically encumbered formazan **Fza**, which has 2,6-dimethylphenyl groups as the N-aryl substituents. Our hypothesis was that the increased steric bulk would result in exclusive formation of the five-member chelate isomer, since that binding mode relieves steric crowding between the N-aryl ring and the cyclometalated aryl. We previously observed this five-member chelate in both cyano-substituted diarylformazanates related to **Fza** and **Fzb**, as well as triarylformazanates where a third aryl ring is present in place of the cyano group. Thus we don't think the cyano group is critical for the adoption of the five-member chelate "open" form, and we wanted to employ **Fza** and **Fzb** to investigate steric effects in the coordination chemistry.

We initially treated the chloro-bridged dimers [Ir(C[^]N)₂(μ-Cl)]₂, where C[^]N is the cyclometalating ligand 2-phenylpyridine (ppy) or 2-(2,4-difluorophenyl)pyridine (F₂ppy), with

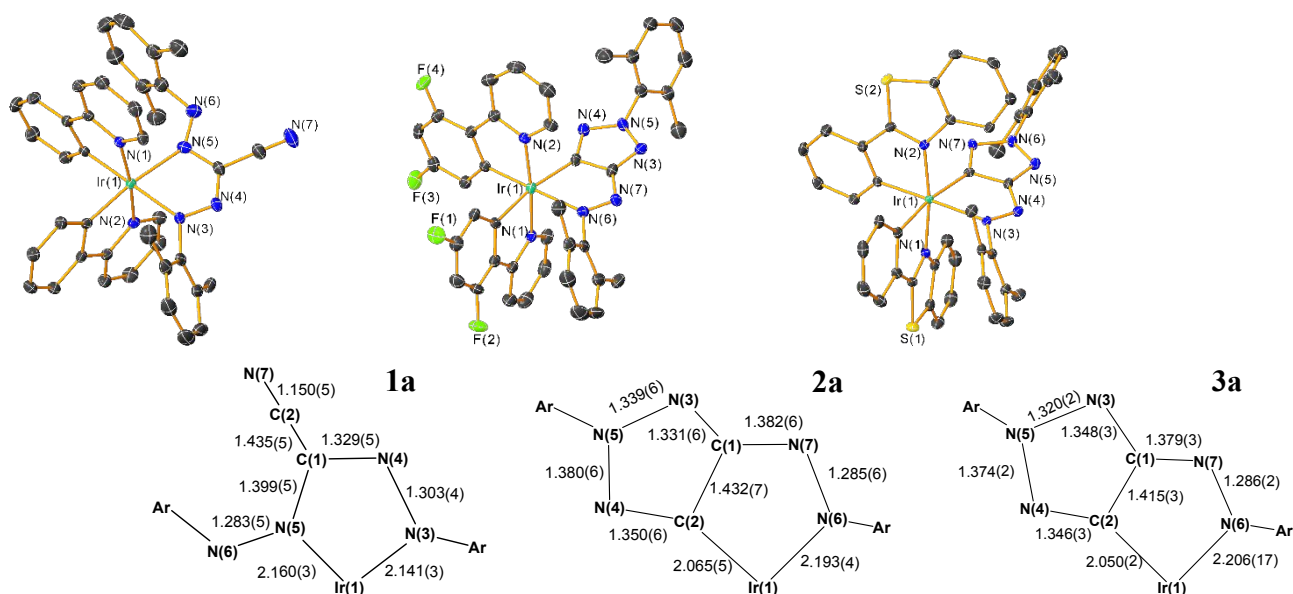


Fig. 1. X-ray crystal structure of complexes **1a**, **2a** and **3a**, with ellipsoids shown at the 50% probability level and hydrogen atoms omitted. To better visualize the geometric differences, the bottom stick diagrams show bond lengths in Å, with esd values in parentheses.

stoichiometric amounts of **Fza** in refluxing ethanol with excess triethylamine. Both of these reactions gave high yields of products with ^1H and $^{13}\text{C}\{^1\text{H}\}$ NMR spectra consistent with C_1 -symmetric complexes, but close inspection of the NMR spectra shows some key differences. Unlike product **1a**, product **2a** only has 3 CH_3 resonances in its ^1H and $^{13}\text{C}\{^1\text{H}\}$ NMR spectra, consistent with free rotation of one of the 2,6-dimethylphenyl rings. In addition, the $^{13}\text{C}\{^1\text{H}\}$ NMR spectrum of **2a** includes a downfield resonance at 179.0 ppm not present in **1a**, and the characteristic $\text{C}\equiv\text{N}$ stretching frequency in the IR spectrum, which occurs at 2206 cm^{-1} in complex **1a**, is completely absent in complex **2a**. As unequivocally established by X-ray crystallography (see below), complex **1a** is the usual five-member chelate iridium formazanate complex, whereas **2a** is a cyclized arylazo-triazolide complex. Cyclization in **2a** ($\text{C}^{\wedge}\text{N} = \text{F}_2\text{ppy}$) but not in **1a** ($\text{C}^{\wedge}\text{N} = \text{ppy}$) suggests electronic effects may be important, since the steric profiles of these two $\text{C}^{\wedge}\text{N}$ ligands are nearly identical but F_2ppy is more electron-poor. To investigate steric effects in the cyclization reaction, we explored modifications to both the cyclometalating and formazanate ligands. First, the formazan **Fza** was paired with two different cyclometalating ligands, 2-phenylbenzothiazole (bt) and 2-phenylthiazole (pta), which on the basis of electrochemistry (see below) are very similar electronically, but sterically are quite different on account of the fused benzo in bt, which “hangs over” the cleft where the formazanate ancillary ligand binds. Spectroscopic and crystallographic analysis clearly indicate that cyclization of the formazanate to the triazolide occurs in the more sterically encumbered complex **3a**, but in **4a** the formazanate does not cyclize, suggesting that cyclization is preferred in a more crowded steric environment. Finally, the isomeric formazan **Fzb**, with 2,4-dimethylphenyl substituents, was also subjected to the same reaction conditions. **Fzb** was partnered with the three $\text{C}^{\wedge}\text{N}$ ligands ppy, F_2ppy , and bt, and in all cases only the formazanate products were obtained, **1b–3b**.

All three of these products give a characteristic $\text{C}\equiv\text{N}$ stretching band in their IR spectra, and the downfield $^{13}\text{C}\{^1\text{H}\}$ NMR signal attributed to the triazolide is absent in each case. Thus, by relieving steric pressure in the formazan ligand, only the uncyclized formazanate products were obtained.

Crystal Structures

The structures of complexes **1a**, **2a** and **3a** were confirmed by single-crystal X-ray diffraction, and are shown in Fig. 1. Refinement data is summarized in Table S2, with bond lengths and bond angles summarized in Table 1 and S3. As is usually the case for bis-cyclometalated iridium complexes, the nitrogen atoms of the two $\text{C}^{\wedge}\text{N}$ ligands are trans to one another, and all three complexes have very similar bond metrics associated with the $\text{C}^{\wedge}\text{N}$ ligands, namely the $\text{Ir}-\text{C}^{\wedge}\text{N}$ and $\text{Ir}-\text{N}^{\wedge}\text{C}$ bond distances ($2.012(5)$ – $2.086(2)$ Å) as well as the $\text{C}^{\wedge}\text{N}$ chelate angles, which span from $78.19(8)^\circ$ to $80.01(13)^\circ$.

Formazanate complex **1a** has a structure reminiscent of several other “open form” cyclometalated iridium complexes recently reported by our group.⁵⁵ Like these previous examples, for complex **1a** the π electrons on the formazanate backbone are primarily localized on the $\text{C}1-\text{N}4$ and $\text{N}5-\text{N}6$ bonds, significantly shorter than the $\text{C}1-\text{N}5$ and $\text{N}3-\text{N}4$ bonds. Similarly, in complexes **2a** and **3a**, the $\text{N}6-\text{N}7$ azo bond distances ($1.285(6)$ Å and $1.286(2)$ Å, respectively), suggest a non-radical azo group. In the 1,2,3-triazolide ring, the $\text{C}1-\text{N}3$ ($1.331(6)$ Å and $1.348(3)$ Å) and $\text{C}2-\text{N}4$ ($1.350(6)$ Å and $1.346(3)$ Å) distances are consistent with imine-like $\text{C}=\text{N}$ double-bond character, whereas the $\text{N}4-\text{N}5$ distances are closer to $\text{N}-\text{N}$ single-bond distances, suggesting the π electrons are not fully delocalized over the five-membered aromatic ring.

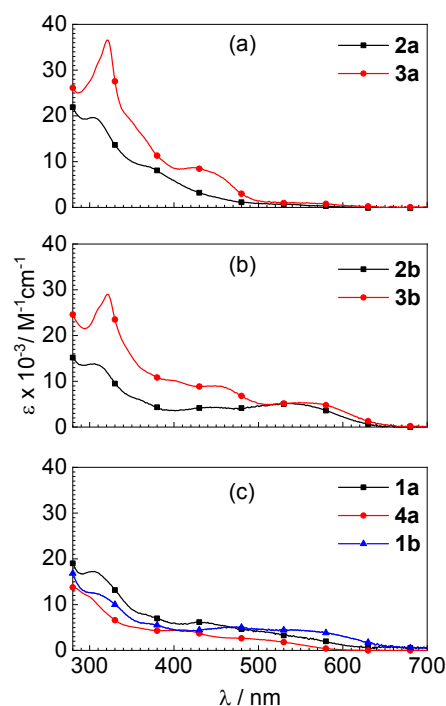
Table 1. Summary of crystallographic bond lengths (Å) and angles (deg) for complex **2a** and **3a**.

| | 2a | 3a |
|-----------|-----------|-----------|
| d (Ir–N6) | 2.193(4) | 2.206(17) |
| d (Ir–C2) | 2.065(5) | 2.050(2) |
| d (N6–N7) | 1.285(6) | 1.286(2) |
| d (N7–C1) | 1.382(6) | 1.379(3) |
| d (C1–C2) | 1.432(7) | 1.415(3) |
| d (C1–N3) | 1.331(6) | 1.348(3) |
| d (C2–N4) | 1.350(6) | 1.346(3) |
| d (N3–N5) | 1.339(6) | 1.320(2) |
| d (N4–N5) | 1.380(6) | 1.374(2) |
| ∠C2–Ir–N6 | 75.53(17) | 74.91(7) |

UV–Vis Absorption Spectroscopy

The colors of the triazolide and formazanate complexes are visually distinguishable, with triazolides **2a** and **3a** exhibiting a dark orange color in solution while the other formazanate complexes are dark red or purple in solution, similar to the free formazans. UV-Vis spectra for the complexes are shown in Fig. 2, with a summary of the data in Table 2. The plots in Fig. 2 are arranged to easily discern differences between the triazolide complexes and the related formazanate complexes. Fig. 2a shows the two triazolide complexes **2a** and **3a**, and the analogous **Fzb** complexes **2b** and **3b**, which have the same C^N ligands, are shown directly below in Fig. 2b. The spectra of the remaining three formazanate complexes are overlaid in Fig. 2c.

In addition to intense peaks in the UV ($\lambda < 350$ nm) attributed to localized $\pi \rightarrow \pi^*$ transitions of the aryl substituents from both C^N and formazanate/4-azo-1,2,3-triazolide ligands, a notable absorption between 480 nm and 600 nm stands out among the 3-cyanodiarylformazanate complexes, which is assigned as a $\pi \rightarrow \pi^*$ within formazanate framework with minimal Ir(d) $\rightarrow \pi^*$ metal-to-ligand-charge transfer (MLCT), in accord with the diarylformazanate Ir(III) complexes we reported recently.⁵⁵ All formazanate complexes show significant visible absorption, and two overlapping visible absorption bands. That said, in **Fzb** complexes the low-energy band (between 536 and 557 nm) is more pronounced and has a discernible maximum, compared to **Fza** complexes where the low-energy band is an ill-defined shoulder. The differences in visible absorption profile between **Fza** and **Fzb** complexes may be due to the larger steric profile of **Fza**, which hinders the rotation of the aryl substituents and decreases the conjugation between the formazanate backbone and the aryl rings. That said, while the absorption profiles are only subtly different for **Fza** and **Fzb** complexes, there are large differences observed for triazolide complexes **2a** and **3a**. In

**Fig. 2.** Overlaid electronic absorption spectra of (a) triazolide complexes **2a** and **3a**, (b) analogous **Fzb** complexes **2b** and **3b**, and (c) the remaining formazanate complexes **1a**, **4a**, and **1b**. Spectra were recorded in tetrahydrofuran (THF) solution at room temperature. Data was collected in intervals of 1 nm, and symbols are included on each plot are to help distinguish the overlaid spectra.**Table 2.** Summary of UV-Vis absorption data recorded in tetrahydrofuran (THF) at room temperature.

| | λ / nm ($\epsilon \times 10^{-3} / \text{M}^{-1}\text{cm}^{-1}$) |
|-----------|-----------------------------------------------------------------------------------|
| 1a | 305 (18), 434 (6.2) |
| 2a | 306 (20), 369 (sh) (8.9) |
| 3a | 321 (37), 430 (8.4) |
| 4a | 413 (4.4), 509 (sh) (2.3) |
| 1b | 309 (sh) (12), 469 (5.0), 542 (sh) (4.2) |
| 2b | 306 (14), 439 (4.3), 536 (5.0) |
| 3b | 321 (29), 402 (sh) (10), 453 (8.9), 557 (5.4) |

these complexes there is comparatively little visible absorption, with multiple overlapping bands blue and near-UV regions, 380–430 nm. The absorption profile of **F₂ppy** complex **2a** does tail to longer wavelengths than is often observed for other neutral bis-cyclometalated iridium complexes with the same cyclometalating ligand,^{59,60} suggesting some visible absorption of the azo-triazolide ancillary ligand, but it is clear that the formazanates are much stronger visible chromophores than their triazolide isomers. UV-Vis spectra were also recorded in three solvents of varying polarity (toluene, THF, and MeOH), shown in Fig. S19, with a summary of data in Table S4, and for all only small spectral differences (<10 nm) are observed in the

different solvents, which indicates very minimal charge-transfer character in the UV-Vis absorption bands. None of the compounds reported here are luminescent at room temperature.

Electrochemistry

The redox properties of all the complexes were evaluated by cyclic voltammetry, with overlaid voltammograms shown in Fig. 3 and redox potentials summarized in Table 3. Each complex shows both oxidation and reduction features within the accessible electrochemical window. In all cases the reduction peaks are electrochemically reversible and oxidation waves are mostly reversible, although in some cases the ratio of the cathodic return current to the anodic current ($i_{p,c}/i_{p,a}$) is less than 1, indicating the features are not completely reversible. This is most clearly apparent in **3a**, where an additional cathodic wave is observed on the return sweep after oxidation, and in **1a** and **4a** where the oxidation is clearly not fully reversible. The potentials of all redox events are responsive to the substitution pattern of C^N and formazanate/azo-triazolide ligands, such that complexes with electron withdrawing groups are easier to reduce but harder to oxidize than the congeners with electron donating groups. For example, replacing the ppy C^N ligand in **1b** with a F₂ppy ligand in **2b** results in a 180 mV anodic shift of the reduction wave and a 220 mV shift of the oxidation wave, owing to the electron-withdrawing effect of the fluorine atoms in F₂ppy.

The separation between the reduction and oxidation potentials for the formazanate complexes, i.e. the electrochemical HOMO–LUMO gap, does seem to depend on the structure of the formazanate. Complexes of **Fza** exhibit separations of 2.51 V (**1a**) and 2.49 V (**4a**), whereas those for **Fzb** complexes are significantly smaller and span a narrow range of 2.28–2.33 V. Consistent with this observation, as noted above **Fzb** complexes have low-energy absorption bands, likely HOMO→LUMO in nature, which are red-shifted compared to the **Fza** complexes. For triazolide complexes **2a** and **3a** the electrochemical features are not drastically different than the

formazanate complexes. The reduction potentials are quite similar, whereas the oxidation potentials are slightly more positive than the potentials for the respective **Fzb** complexes that have the same C^N ligands (**2b** and **3b**). The electrochemical HOMO–LUMO gaps in the triazolide complexes all fall in the range spanned by the formazanate complexes, suggesting that the frontier orbital energies of the azo-triazolide complexes are not substantially different from their formazanate relatives, even though the UV-Vis absorption spectra are markedly different (see Fig. 2).

Table 3. Summary of electrochemical data for complexes **1a–4a**, **1b–3b**.

| | E^{ox} (V) | E^{red} (V) |
|-----------|---------------------|----------------------|
| 1a | 0.66 | -1.85 |
| 2a | 0.84 | -1.76 |
| 3a | 0.66 | -1.82 |
| 4a | 0.61 | -1.88 |
| 1b | 0.46 | -1.82 |
| 2b | 0.68 | -1.64 |
| 3b | 0.49 | -1.84 |

Although the redox potentials of the complexes described here fall into a relatively narrow range, owing to the rather similar substituent patterns of the formazanate and azo-triazolide ligands, we can make tentative electrochemical assignments based on analogies with other cyclometalated iridium complexes, with and without formazanate ancillary ligands. The complexes described here have similar reduction potentials to cyclometalated iridium formazanate complexes⁵⁵ and are all significantly easier to reduce than bis-cyclometalated iridium complexes where the LUMO resides on the C^N ligand,^{61,62} suggesting that the first reduction occurs on the formazanate or azo-triazolide ancillary ligand. This observation indicates that, like formazanates, the isomeric azo-triazolides introduced here are also redox-active. Assignment of the oxidation waves is less clear from the data available here, and likely involves a HOMO that is delocalized with mixed contribution from Ir, the C^N ligand, and the formazanate/azo-triazolide ancillary ligand, a contention supported by DFT calculations (see below). We do note that in more electronically diverse iridium formazanate complexes we prepared previously, the oxidation potential was quite sensitive to the formazanate substitution, suggesting the HOMO has significant contribution from the formazanate. That said, the potentials of the complexes described here are not atypical for neutral bis-cyclometalated iridium complexes and are quite responsive to fluorination of the C^N ligand (see **2a** and **2b** in Table 3), so it is likely that the HOMO in these compounds also includes significant Ir-aryl character, as is normal for cyclometalated iridium complexes.⁶³ We also characterized the redox

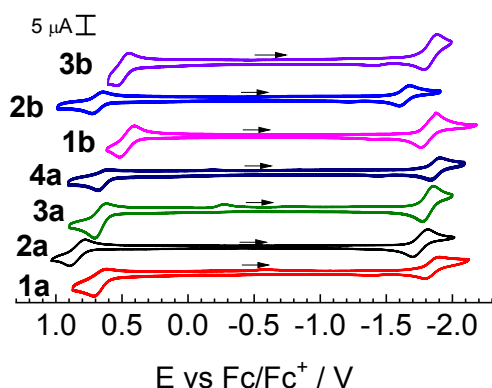


Fig. 3. Overlaid cyclic voltammograms of complexes **1a–4a** and **1b–3b**. CVs were recorded in CH₂Cl₂ with 0.1 M NBu₄PF₆ supporting electrolyte, using a glassy carbon working electrode and a scan rate of 0.1 V/s. The arrows indicate the scan direction.

behaviors of all the complexes in an extended scan window, shown in Fig.

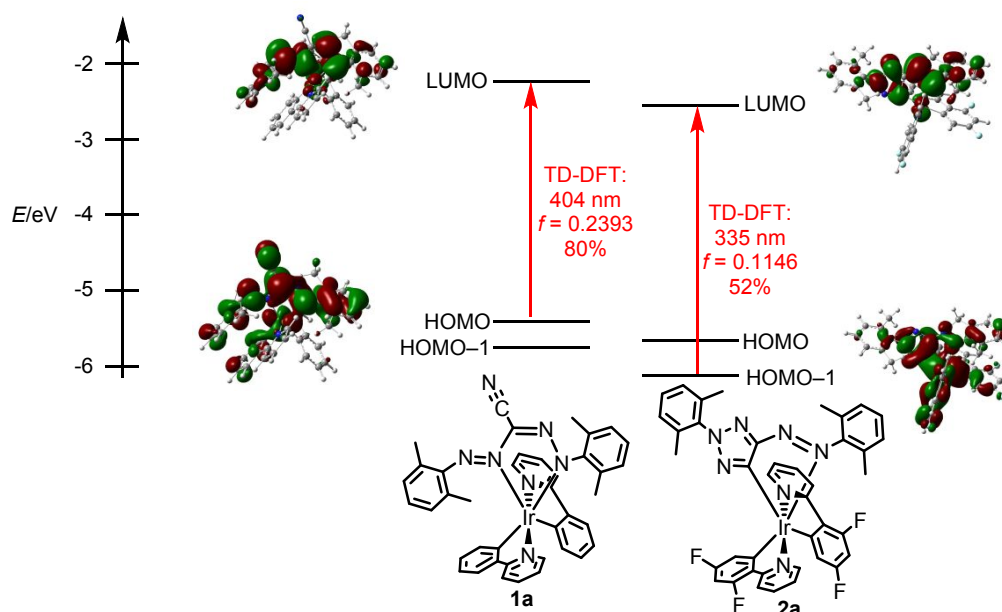


Fig. 4. Summary of DFT results for complexes **1a** and **2a**. The chemical structures show the orientation of the molecules in the orbital contour plots, with a “front-facing” orientation of the formazanate or triazolide ligand. Frontier orbital energies are indicated, and the red arrow shows the transition that is the major contributor to the lowest-energy singlet state, with the computed wavelength and oscillator strength shown. The percent contribution of that one-electron transition to the excited state is also shown, and contour plots (0.02 au) depict the orbitals that are principally involved, HOMO and LUMO for **1a**, HOMO-1 and LUMO for **2a**.

S20 and summarized in Table S5. For all the complexes, additional irreversible oxidation peaks were observed, and in most cases oxidation by >1 electron results in the first oxidation also becoming irreversible. Additional reduction peaks were observed only in complexes **1b** and **2b**. For other complexes, no additional reduction peak was detected within the dichloromethane solvent window.

DFT Calculations

Molecular geometries for four compounds related to this study were optimized in the gas phase, using the B3LYP-D3 functional with 6-311G(d,p) basis set for non-metal atoms and SDD basis set for Ir. Chart 1 shows the structures of these four compounds. The computed compounds are Ir(ppy)₂(Fza) (**1a**) and its unobserved triazolide analogue **1a'**, and triazolide compound **2a** and the unobserved formazanate analogue Ir(F₂ppy)₂(Fza) (**2a'**). For **1a** and **2a**, the optimized geometries are a good match for the crystal structures, with very similar bond lengths, bond angles, and ligand conformations observed. For unobserved products **1a'** and **2a'**, the structural metrics are in line with the

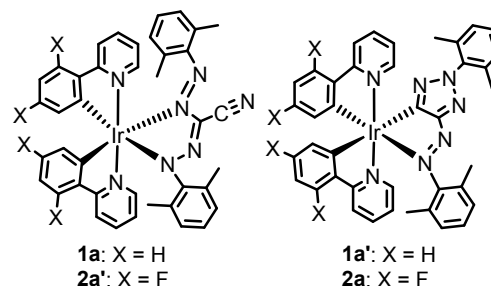


Chart 1. Structures of compounds evaluated by DFT methods.

other characterized triazolide and formazanate complexes. In the gas phase, DFT predicts that in both cases the uncyclized formazanate isomer is the more stable species, by ~13 kcal/mol in each case. This result is consistent with the outcome when C[^]N = ppy, where formazanate complex **1a** is observed as the exclusive product, but is at odds with the outcome when C[^]N = F₂ppy. Since DFT optimizations were run in the gas phase we also did a single-point calculation with implicit EtOH solvation, the solvent used during synthesis, and the energy landscape was not significantly altered.

This anomalous outcome led us to consider the possibility that the product selectivity was driven by solubility, since reactions conducted in EtOH always lead to precipitation of the product. To test this, we repeated the syntheses of triazolide complexes **2a** and **3a** in CH₂Cl₂ solvent, conditions we have previously used to synthesize iridium formazanate complexes⁵⁵ during which the product remains in solution during synthesis. However, even under these conditions triazolide complexes **2a**

and **3a** were exclusively isolated, and again the formation of **2a** is at odds with the DFT results. At this stage a clear explanation for this product selectivity is elusive, though the DFT results suggest that **2a** (and by extension, likely **3a**) is not the thermodynamically preferred product, even though it is formed exclusively during the reaction. That said, it is unclear why the identity of the cyclometalating ligand, in particular when changing from ppy to F₂ppy, has such a dramatic effect on the selectivity for formazanate versus triazolide forms.

In spite of the lack of clarity with regards to product selectivity, DFT results give a clear picture of the electronic structure and are consistent with the CV and UV-vis spectroscopic measurements described above. Fig. 4 above summarizes some of the key DFT results, showing frontier orbital energies for both **1a** and **2a**. In addition, TD-DFT, calculated using the TD-M06-2X functional with the same atomic basis sets, was used to compute the lowest-energy UV-vis transition. TD-DFT results, showing the computed transition wavelengths and the orbitals that constitute the major one-electron transition for each excited state, are also summarized in Fig. 4. CV results described above predicted rather similar frontier orbital energies and HOMO–LUMO gaps for **1a** and **2a**, trends that are reproduced well by DFT. The experimentally determined HOMO–LUMO gaps for **2a** is <0.1 eV larger than **1a**, and DFT calculations predict that the HOMO–LUMO gap for **2a** is slightly smaller, by 0.02 eV. The frontier orbitals for both **1a** and **2a** are primarily ligand-centered π and π^* orbitals residing on the formazanate or triazolide ligand.

Both experiment and theory are consistent with the idea that **1a** and **2a** have very similar HOMO–LUMO gaps, but in spite of this similarity the UV-vis spectra (Fig. 2) are quite different, with **1a** having strong visible absorption and **2a** absorbing primarily in the UV and blue regions. This disparity is clearly explained by the TD-DFT results. In both compounds the lowest-energy electronic transition involves substantial configuration interaction, but for **1a** the transition occurs in the visible region ($\lambda = 404$ nm) and has 80% HOMO→LUMO character, and thus is primarily an intraligand $\pi \rightarrow \pi^*$ transition. In contrast, for **2a** the lowest-energy transition occurs at much shorter wavelength ($\lambda = 335$ nm) and has majority (HOMO–1)→LUMO character, and only 5% contribution from the HOMO→LUMO transition. The HOMO–1 orbital in **2a** involves contributions from both the triazolide and F₂ppy ligands, so the (HOMO–1)→LUMO transition can be described as having mixed intraligand and ligand-to-ligand charge transfer character. Thus, the frontier orbital energies are very similar for **1a** and **2a**, but the UV-vis transitions for these two isomers involve different frontier orbitals and thus occur in different parts of the spectrum.

Conclusion

In this work, we disclosed examples of 2-aryl-4-arylaazo-2H-1,2,3-triazolide bis-cyclometalated iridium complexes, formed by cyclization of 3-cyano-1,5-diarylformazanates. In most cases the typical reaction conditions left the formazanate ligand in its uncyclized form, but steric effects on both the formazanate ligand and the cyclometalating ligand appear to be important

for driving the cyclization to the azo-triazolide. The two distinct ligand structures are discernible spectroscopically and unequivocally established by single-crystal X-ray diffraction. A systematic comparison of different C^N and formazanate/4-azo-1,2,3-triazolide ligands reveals that the redox potentials are rather similar within the series of compounds, although the UV-vis absorption profiles are distinct and the triazolide complexes have much less pronounced visible absorption, due to the predominance of (HOMO–1)→LUMO transitions in these complexes versus HOMO→LUMO transitions in the formazanate isomer. In future work we aim to develop a more general route for this new 4-azo-1,2,3-triazolide ligand class and expand the coordination chemistry to other late transition metals.

Experimental section

Materials

Reactions were carried out in a nitrogen atmosphere using standard Schlenk techniques. Solvents, starting materials, and reagents were of commercial origin and used without further purification unless stated otherwise below. Tetrahydrofuran (THF), methanol (MeOH), and toluene for UV-Vis spectroscopy, and dichloromethane (DCM) for electrochemical measurements were dried by the method of Grubbs, passing through dual alumina columns on a commercial solvent purification system (SPS). Tetrabutylammonium hexafluorophosphate (TBAPF₆) was recrystallized from hot ethanol and ferrocene was sublimed at ambient pressure before use in electrochemical experiments. CDCl₃ and CD₃CN for NMR spectroscopy were stored over potassium carbonate and molecular sieves to remove acidic impurities and moisture. The ligand 3-cyano-1,5-bis(2,6-dimethylphenyl)formazan (**Fza**) was prepared by following the literature procedures⁶⁴ and 3-cyano-1,5-bis(2,4-dimethylphenyl)formazan (**Fzb**) was prepared by a modified version described below. The iridium precursors [Ir(ppy)₂(μ -Cl)]₂ (ppy = 2-phenylpyridine), [Ir(F₂ppy)₂(μ -Cl)]₂ (F₂ppy = 2-(2,4-difluorophenyl)pyridine), [Ir(bt)₂(μ -Cl)]₂ (bt = 2-phenylbenzothiazole), and [Ir(pta)₂(μ -Cl)]₂ (pta = 2-phenylthiazole) were prepared by a modified version of the well-known Nonoyama procedure.^{65,66}

Physical methods

NMR spectra were recorded at room temperature using a JEOL ECA-600, ECA-500, or ECA-400 NMR spectrometer. Infrared (IR) spectra were measured using a Thermo Nicolet Avatar FT-IR spectrometer with diamond ATR. UV-vis absorption spectra were recorded in THF, toluene, and MeOH solutions in screw-capped 1 cm quartz cuvettes using an Agilent Cary 8454 UV-vis spectrophotometer. Cyclic voltammetry (CV) measurements were performed with a CH Instruments 602E potentiostat interfaced with a nitrogen glovebox via wire feedthroughs. Samples were dissolved in dichloromethane (CH₂Cl₂) with 0.1 M TBAPF₆ as a supporting electrolyte. A 3 mm diameter glassy carbon working electrode, a platinum wire counter electrode, and a silver wire pseudo-reference electrode were used.

Potentials were referenced to an internal standard of ferrocene. The bulk purity for all complexes is established by elemental analysis, performed by Atlantic Microlab, Inc.

Synthesis of compounds

Ligand Fzb. The title compound was prepared by a modified version of the literature procedures used for related formazanate ligands.⁶⁴ Sodium nitrite (3.0 g, 0.043 mol) was added to a solution of 2,4-dimethylaniline (4.9 mL, 0.040 mmol), 12 M concentrated hydrochloric acid (10 mL) and water (10 mL) at -5°C in small portions over a 10 min period. After 15 min of stirring, the mixture was added to a second solution containing cyanoacetic acid (1.7 g, 0.020 mmol), sodium hydroxide (8.0 g, 0.20 mmol), and water (100 mL) at 0°C over a 30 min period. The reaction completion was confirmed by TLC. The resulting dark red organic layer obtained after biphasic extraction from dichloromethane/water was dehydrated by MgSO_4 and concentrated to dryness. The crude product was purified via column chromatography (neutral alumina stationary phase and dichloromethane eluent), and the eluate was concentrated in vacuo to afford **Fzb** as dark red solid. Yield: 1.3 g (21%). ^1H NMR (400 MHz, CDCl_3): δ 12.22 (s, 1H, NH), 7.58 (d, $J = 8.1$ Hz, 2H, ArH), 7.10 (d, $J = 8.8$ Hz, 4H, ArH), 2.50 (s, 6H, CH_3), 2.35 (s, 6H, CH_3). ^{13}C NMR (151 MHz, CDCl_3): δ 143.0, 139.4, 132.0, 131.7, 128.1, 126.5, 115.9, 114.6, 21.3, 17.7. FT-IR: 3332 (ν_{NH}), 2222 (ν_{CN}), 1527, 1277(m) cm^{-1} . Anal. Calcd for $\text{C}_{18}\text{H}_{19}\text{N}_5$: C, 70.80, H, 6.27, N, 22.93. Found: C, 70.85, H, 6.13, N, 23.02.

Complex 1a. $[\text{Ir}(\text{ppy})_2(\mu\text{-Cl})]_2$ (54 mg, 0.050 mmol) and **Fza** (30 mg, 0.10 mmol) were combined in ethanol (10 mL) with excess triethylamine (0.1 mL), and the mixture was deoxygenated under the protection of N_2 . The mixture was refluxed for 36 h. A red precipitate was observed at the bottom of the flask after the reaction was completed. Solvent was removed by filtration, and the solid was re-crystallized from CH_2Cl_2 and pentane to purify the product, which was crystallized again by vapor diffusion of pentane into a concentrated CHCl_3 solution. Yield: 65 mg (74%). ^1H NMR (500 MHz, CDCl_3): δ 8.53 (d, $J = 4.7$ Hz, 1H, ArH), 8.39 (d, $J = 4.7$ Hz, 1H, ArH), 7.81 (t, $J = 7.6$ Hz, 1H, ArH), 7.75 (t, $J = 7.5$ Hz, 1H, ArH), 7.68 (d, $J = 8.1$ Hz, 1H, ArH), 7.54 (d, $J = 8.1$ Hz, 1H, ArH), 7.13 (d, $J = 6.6$ Hz, 3H, ArH), 6.96 (d, $J = 7.4$ Hz, 1H, ArH), 6.67 (t, $J = 7.2$ Hz, 1H, ArH), 6.61–6.52 (m, 2H, ArH), 6.52–6.43 (m, 2H, ArH), 6.43–6.34 (m, 3H, ArH), 6.29 (d, $J = 7.2$ Hz, 1H, ArH), 6.21 (d, $J = 7.1$ Hz, 1H, ArH), 5.85 (d, $J = 7.5$ Hz, 1H, ArH), 5.76 (d, $J = 7.4$ Hz, 1H, ArH), 2.14 (s, 3H, CH_3), 1.99 (s, 3H, CH_3), 1.36 (s, 3H, CH_3), 1.11 (s, 3H, CH_3). ^{13}C NMR (151 MHz, CDCl_3): δ 169.8, 167.8, 152.7, 152.6, 152.3, 149.6, 149.4, 146.7, 142.8, 142.4, 137.9, 137.7, 134.6, 132.8, 131.7, 131.3, 130.4, 129.1, 128.6, 128.5, 128.4, 128.2, 127.6, 126.9, 126.3, 126.2, 125.7, 124.3, 122.7, 122.1, 121.8, 121.5, 120.8, 119.3, 119.2, 116.2, 22.6, 20.0, 18.2, 16.9. FT-IR: 2206 (ν_{CN}), 1608(m), 1479, 1214 cm^{-1} . Anal. Calcd for $\text{C}_{40}\text{H}_{34}\text{N}_7\text{Ir}$: C, 59.68, H, 4.26, N, 12.18. Found: C, 59.50, H, 4.37, N, 12.09.

Complex 2a. The title compound was prepared by the general method described above for complex **1a**, using $[\text{Ir}(\text{F}_2\text{ppy})_2(\mu\text{-Cl})]_2$ (61 mg, 0.050 mmol) and **Fza** (30 mg, 0.10 mmol), being crystallized by vapor diffusion of pentane into concentrated

ethyl acetate solution. Yield: 70 mg (80%). ^1H NMR (500 MHz, CDCl_3): δ 8.44 (d, $J = 5.5$ Hz, 1H, ArH), 8.25 (d, $J = 8.4$ Hz, 1H, ArH), 7.98 (d, $J = 8.3$ Hz, 1H, ArH), 7.86 (d, $J = 5.6$ Hz, 1H, ArH), 7.71 (dd, $J = 16.6, 8.3$ Hz, 2H, ArH), 7.22 (t, $J = 7.5$ Hz, 1H, ArH), 7.09 (d, $J = 7.5$ Hz, 2H, ArH), 6.95–6.87 (m, 2H, ArH), 6.85 (t, $J = 6.5$ Hz, 1H, ArH), 6.74 (d, $J = 7.4$ Hz, 1H, ArH), 6.65 (d, $J = 7.2$ Hz, 1H, ArH), 6.32 (t, $J = 10.9$ Hz, 1H, ArH), 6.19 (t, $J = 10.7$ Hz, 1H, ArH), 6.03 (d, $J = 7.4$ Hz, 1H, ArH), 5.57 (d, $J = 9.3$ Hz, 1H, ArH), 2.12 (s, 3H, CH_3), 1.92 (s, 6H, CH_3), 1.13 (s, 3H, CH_3). ^{19}F NMR (470 MHz, CDCl_3): δ -108.6 (s, 1F), -109.5 (s, 1F), -110.6 (s, 1F), -110.9 (s, 1F). ^{13}C NMR (151 MHz, CDCl_3): δ 179.0, 173.6, 172.7, 170.0, 167.1, 164.3, 163.7, 162.1, 162.0, 155.1, 153.8, 150.6, 150.3, 140.3, 138.0, 136.7, 135.5, 130.8, 130.1, 129.6, 128.4, 128.2, 128.2, 128.1, 127.8, 126.3, 123.2, 122.9, 122.7, 120.5, 115.1, 111.7, 97.8, 96.9, 21.3, 17.5, 16.9. FT-IR 1597(m), 1474(m), 1289(m) cm^{-1} . Anal. Calcd for $\text{C}_{40}\text{H}_{30}\text{N}_7\text{F}_4\text{Ir}$: C, 54.79, H, 3.45, N, 11.18. Found: C, 54.98, H, 3.61, N, 10.94.

Complex 3a. The title compound was prepared by the general method described above for complex **1a**, using $[\text{Ir}(\text{bt})_2(\mu\text{-Cl})]_2$ (65 mg, 0.050 mmol) and **Fza** (30 mg, 0.10 mmol), being crystallized by vapor diffusion of pentane into concentrated ethyl acetate solution. Yield: 70 mg (76%). ^1H NMR (600 MHz, CDCl_3): δ 7.78 (d, $J = 7.9$ Hz, 3H, ArH), 7.64 (d, $J = 7.6$ Hz, 1H, ArH), 7.34 (t, $J = 7.5$ Hz, 1H, ArH), 7.25 (t, $J = 7.5$ Hz, 1H, ArH), 7.20–7.10 (m, 4H, ArH), 7.02 (d, $J = 7.7$ Hz, 3H, ArH), 6.87 (t, $J = 7.3$ Hz, 1H, ArH), 6.82–6.71 (m, 5H, ArH), 6.52 (t, $J = 7.5$ Hz, 1H, ArH), 6.44 (d, $J = 7.2$ Hz, 1H, ArH), 6.13 (d, $J = 7.8$ Hz, 1H, ArH), 2.02 (s, 3H, CH_3), 1.78 (s, 6H, CH_3), 0.98 (s, 3H, CH_3). ^{13}C NMR (151 MHz, CDCl_3): δ 183.2, 180.1, 178.4, 170.2, 169.7, 151.1, 150.5, 150.2, 149.9, 141.4, 140.4, 139.5, 138.4, 135.5, 134.3, 133.2, 131.5, 131.4, 131.0, 130.8, 130.5, 129.7, 129.4, 128.4, 128.2, 128.0, 127.8, 127.2, 126.22, 126.18, 125.6, 124.9, 124.1, 122.5, 122.2, 121.9, 120.7, 120.5, 23.2, 17.2, 17.0. FT-IR: 1582(m), 1434(m), 1295(m) cm^{-1} . Anal. Calcd for $\text{C}_{44}\text{H}_{34}\text{N}_7\text{S}_2\text{Ir}$: C, 57.62, H, 3.74, N, 10.69. Found: C, 57.72, H, 3.87, N, 10.44.

Complex 4a. The title compound was prepared by the general method described above for complex **1a**, using $[\text{Ir}(\text{pta})_2(\mu\text{-Cl})]_2$ (55 mg, 0.050 mmol) and **Fza** (30 mg, 0.10 mmol). Yield: 56 mg (69%). ^1H NMR (500 MHz, CDCl_3): δ 7.74 (d, $J = 3.3$ Hz, 1H, ArH), 7.63 (d, $J = 3.4$ Hz, 1H, ArH), 7.38 (dd, $J = 10.0, 3.3$ Hz, 2H, ArH), 7.01 (d, $J = 7.3$ Hz, 1H, ArH), 6.97 (d, $J = 7.6$ Hz, 1H, ArH), 6.72 (t, $J = 7.4$ Hz, 1H, ArH), 6.67 (d, $J = 7.4$ Hz, 1H, ArH), 6.57 (t, $J = 7.3$ Hz, 1H, ArH), 6.54–6.42 (m, 5H, ArH), 6.39 (t, $J = 7.5$ Hz, 1H, ArH), 6.17 (d, $J = 7.4$ Hz, 1H, ArH), 5.91 (d, $J = 7.6$ Hz, 1H, ArH), 5.81 (d, $J = 7.0$ Hz, 1H, ArH), 2.10 (s, 3H, CH_3), 2.09 (s, 3H, CH_3), 1.45 (s, 3H, CH_3), 1.39 (s, 3H, CH_3). ^{13}C NMR (126 MHz, CDCl_3): δ 181.5, 179.4, 151.0, 149.4, 149.3, 145.7, 142.3, 142.2, 138.9, 138.7, 135.1, 132.6, 131.7, 131.5, 130.8, 129.3, 129.2, 128.5, 128.3, 128.1, 127.5, 126.9, 126.7, 126.5, 125.8, 124.7, 123.3, 122.1, 121.1, 117.3, 116.8, 115.9, 22.0, 19.8, 17.9, 17.2. FT-IR: 2207 (ν_{CN}), 1582, 1438, 1216. Anal. Calcd for $\text{C}_{36}\text{H}_{30}\text{N}_7\text{S}_2\text{Ir}$: C, 52.92, H, 3.70, N, 12.00. Found: C, 52.87, H, 3.91, N, 11.93.

Complex 1b. $[\text{Ir}(\text{ppy})_2(\mu\text{-Cl})]_2$ (54 mg, 0.050 mmol) and **Fzb** (30 mg, 0.10 mmol) were combined in ethanol (10 mL) with excess triethylamine (0.1 mL), and the mixture was deoxygenated under the protection of N_2 . The mixture was refluxed for 36 h and the color changed from dark red to purple. The reaction

completion was confirmed by TLC. Solvent was removed using rotary evaporation, and the product was re-dissolved in a minimum amount of ethyl acetate. After that column chromatography (hexane / ethyl acetate gradient eluent, neutral alumina) was performed to purify the product. Yield: 65 mg (74%). ^1H NMR (500 MHz, CDCl_3): δ 8.50 (d, $J = 5.6$ Hz, 1H, ArH), 8.41 (d, $J = 5.6$ Hz, 1H, ArH), 7.79 (t, $J = 7.7$ Hz, 1H, ArH), 7.73 (dd, $J = 14.4, 7.8$ Hz, 2H, ArH), 7.58 (d, $J = 8.1$ Hz, 1H, ArH), 7.13 (td, $J = 13.2, 6.5$ Hz, 3H, ArH), 7.06 (d, $J = 7.3$ Hz, 1H, ArH), 6.58 (dt, $J = 14.8, 7.6$ Hz, 4H, ArH), 6.43–6.35 (m, 3H, ArH), 6.32 (d, $J = 8.1$ Hz, 1H, ArH), 6.02 (d, $J = 7.7$ Hz, 1H, ArH), 5.91 (d, $J = 7.8$ Hz, 1H, ArH), 5.88 (d, $J = 7.2$ Hz, 1H, ArH), 5.81 (d, $J = 7.6$ Hz, 1H, ArH), 2.06 (s, 3H, CH_3), 1.99 (s, 3H, CH_3), 1.74 (s, 3H, CH_3), 1.60 (s, 3H, CH_3). ^{13}C NMR (151 MHz, CDCl_3) δ 169.1, 167.6, 155.4, 151.09, 151.06, 150.5, 148.9, 148.3, 148.0, 143.0, 142.2, 137.5, 137.3, 136.6, 134.8, 132.2, 131.2, 130.9, 130.8, 130.5, 129.5, 129.4, 129.2, 126.2, 125.3, 124.5, 124.1, 123.5, 122.5, 122.2, 121.6, 119.9, 119.2, 119.1, 118.5, 116.5, 29.8, 18.2, 17.3, 17.3. FT-IR: 2202 (ν_{CN}), 1607(m), 1476, 1224(m) cm^{-1} . Anal. Calcd for $\text{C}_{40}\text{H}_{34}\text{N}_7\text{Ir}$: C, 59.68, H, 4.26, N, 12.18. Found: C, 59.64, H, 4.27, N, 11.99.

Complex 2b. The title compound was prepared by the general method described above for complex **1b**, using $[\text{Ir}(\text{F}_2\text{ppy})_2(\mu\text{-Cl})_2]$ (61 mg, 0.050 mmol) and **Fzb** (30 mg, 0.10 mmol). Yield: 60 mg (68%). ^1H NMR (500 MHz, CDCl_3): δ 8.47 (d, $J = 5.3$ Hz, 1H, ArH), 8.39 (d, $J = 5.4$ Hz, 1H, ArH), 8.12 (d, $J = 8.3$ Hz, 1H, ArH), 7.99 (d, $J = 8.3$ Hz, 1H, ArH), 7.88 (t, $J = 7.9$ Hz, 1H, ArH), 7.82 (t, $J = 7.9$ Hz, 1H, ArH), 7.2 (dt, $J = 23.0, 6.3$ Hz, 2H, ArH), 6.64 (s, 1H, ArH), 6.55 (s, 1H, ArH), 6.41 (d, $J = 8.0$ Hz, 1H, ArH), 6.38 (d, $J = 8.1$ Hz, 1H, ArH), 6.21 (d, $J = 7.7$ Hz, 1H, ArH), 6.18–6.06 (m, 2H, ArH), 5.89 (d, $J = 7.7$ Hz, 1H, ArH), 5.30 (d, $J = 8.5$ Hz, 1H, ArH), 5.25 (d, $J = 8.5$ Hz, 1H, ArH), 2.11 (s, 3H, CH_3), 2.08 (s, 3H, CH_3), 1.67 (s, 3H, CH_3), 1.53 (s, 3H, CH_3). ^{19}F NMR (470 MHz, CDCl_3): δ -107.2 (q, $J = 9.3$ Hz, 1F), -108.7 (q, $J = 9.3$ Hz, 1F), -109.9 (t, $J = 11.5$ Hz, 1F), -110.2 (t, $J = 11.4$ Hz, 1F). ^{13}C NMR (151 MHz, CDCl_3): δ 165.5, 164.1, 163.6, 163.4, 161.9, 161.7, 161.3, 160.1, 159.6, 159.1, 152.1, 151.1, 150.5, 149.0, 147.4, 138.7, 138.5, 137.3, 135.6, 134.5, 131.5, 130.8, 129.6, 126.9, 125.8, 125.4, 124.0, 123.4, 123.3, 123.0, 122.7, 118.5, 115.7, 114.2, 113.1, 98.1, 96.4, 20.9, 20.7, 17.9, 17.2. FT-IR: 2213 (ν_{CN}), 1738, 1601(m), 1402, 1228(m) cm^{-1} . Anal. Calcd for $\text{C}_{40}\text{H}_{30}\text{N}_7\text{F}_4\text{Ir}$: C, 54.79, H, 3.45, N, 11.18. Found: C, 54.93, H, 3.40, N, 11.02.

Complex 3b. The title compound was prepared by the general method described above for complex **1b**, using $[\text{Ir}(\text{bt})_2(\mu\text{-Cl})_2]$ (65 mg, 0.050 mmol) and **Fzb** (30 mg, 0.10 mmol). Yield: 40 mg (44%). ^1H NMR (500 MHz, CDCl_3): δ 7.92 (d, $J = 8.0$ Hz, 1H, ArH), 7.88 (t, $J = 8.2$ Hz, 2H, ArH), 7.73 (d, $J = 8.1$ Hz, 1H, ArH), 7.63 (t, $J = 7.7$ Hz, 1H, ArH), 7.54 (t, $J = 7.6$ Hz, 1H, ArH), 7.49–7.41 (m, 2H, ArH), 7.12 (d, $J = 7.6$ Hz, 1H, ArH), 7.05 (d, $J = 7.6$ Hz, 1H, ArH), 6.64 (q, $J = 7.0$ Hz, 2H, ArH), 6.56 (dd, $J = 14.0, 6.0$ Hz, 2H, ArH), 6.54–6.49 (m, 2H, ArH), 6.44 (d, $J = 7.9$ Hz, 1H, ArH), 6.37 (d, $J = 8.1$ Hz, 1H, ArH), 6.19 (d, $J = 8.1$ Hz, 1H, ArH), 6.09 (d, $J = 7.7$ Hz, 1H, ArH), 6.03 (d, $J = 7.7$ Hz, 1H, ArH), 5.86 (d, $J = 7.9$ Hz, 1H, ArH), 2.06 (s, 3H, CH_3), 2.03 (s, 3H, CH_3), 1.43 (s, 3H, CH_3), 1.33 (s, 3H, CH_3). ^{13}C NMR (151 MHz, CDCl_3): δ 181.8, 180.3, 158.2, 149.5, 149.5, 148.8, 147.3, 147.0, 139.2, 138.9, 136.8,

136.1, 134.7, 133.1, 131.7, 131.6, 131.3, 131.2, 131.1, 131.0, 130.8, 130.6, 129.1, 128.6, 128.4, 126.2, 126.1, 126.0, 125.6, 125.5, 125.24, 125.20, 123.1, 122.6, 122.2, 120.4, 120.3, 119.9, 118.4, 116.2, 21.0, 20.9, 17.7, 17.0. FT-IR: 2205 (ν_{CN}), 1581(m), 1406(m), 1223(m) cm^{-1} . Anal. Calcd for $\text{C}_{44}\text{H}_{34}\text{N}_7\text{S}_2\text{Ir}$: C, 57.62, H, 3.74, N, 10.69. Found: C, 57.78, H, 3.72, N, 10.60.

X-ray Crystallography Details

Single crystals of **1a**, **2a**, and **3a** were grown by diffusing pentane into concentrated chloroform, dichloromethane, or ethyl acetate (EA) solutions. Crystals were mounted on a Bruker Apex II three-circle diffractometer using $\text{MoK}\alpha$ radiation ($\lambda = 0.71073$ Å). The data were collected at 123(2) K and was processed and refined within the APEXII software. Structures were solved by direct methods in SHELXS and refined by standard difference Fourier techniques in the program SHELXL.⁶⁷ Hydrogen atoms were placed in calculated positions using the standard riding model and refined isotropically. All non-hydrogen atoms were refined anisotropically. In the structure of **1a**, one of the two chloroform solvate molecules was modeled as a two-part disorder. Distance restraints were used to affix the 1,2 and 1,3, distances in the disordered parts, and rigid bond restraints (SIMU and DELU) were used for the thermal ellipsoid parameters. Crystallographic details are summarized in Table S2.

Computational Details

Geometry optimizations were performed in the gas phase at the B3LYP-D3 level employing Gaussian16. The 6-311G(d,p) basis set was used for C, H, N, and F, and the SDD basis set with effective core potential (ECP) was used for Ir. Optimized geometries of **1a** and **2a** matched well with the crystal structure. Vibrational frequency calculations verified the nature of the stationary points, indicating that the ground state is a minimum on the potential energy surface. TD-DFT calculations were performed in the gas phase at the M06-2X level using the same basis sets. Optimized Cartesian coordinates are listed in Tables S6–S9.

Acknowledgements

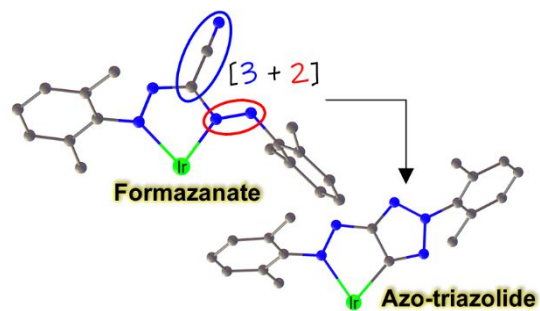
T. S. T acknowledges the University of Houston and the Welch Foundation (Grant no. E-1887) for funding. J. I. W. thanks the National Science Foundation (NSF) (CHE-1751370) National Institute of General Medical Sciences (NIGMS) of the National Institutes of Health (R35GM133548) for grant support, as well as computational resources provided by the uHPC cluster, managed by the University of Houston and acquired through support from the NSF (MRI-1531814).

Notes and references

- 1 Y. Bourne, K. B. Sharpless, P. Taylor and P. Marchot, *J. Am. Chem. Soc.*, 2016, **138**, 1611–1621.
- 2 W. Zhai, B. M. Chapin, A. Yoshizawa, H.-C. Wang, S. A. Hodge, T. D. James, E. V. Anslyn and J. S. Fossey, *Org. Chem. Front.*, 2016, **3**, 918–928.
- 3 L. Türker, *Def. Technol.*, 2016, **12**, 1–15.

- 4 V. V. Rostovtsev, L. G. Green, V. V. Fokin and K. B. Sharpless, *Angew. Chem. Int. Ed.*, 2002, **41**, 2596–2599.
- 5 Y. Qu and S. P. Babailov, *J. Mater. Chem. A*, 2018, **6**, 1915–1940.
- 6 Q.-H. Lin, Y.-C. Li, Y.-Y. Li, Z. Wang, W. Liu, C. Qi and S.-P. Pang, *J. Mater. Chem.*, 2011, **22**, 666–674.
- 7 A. S. Kumar, V. D. Ghule, S. Subrahmanyam and A. K. Sahoo, *Chem. – Eur. J.*, 2013, **19**, 509–518.
- 8 A. Brik, J. Alexandratos, Y.-C. Lin, J. H. Elder, A. J. Olson, A. Wlodawer, D. S. Goodsell and C.-H. Wong, *ChemBioChem*, 2005, **6**, 1167–1169.
- 9 T. Weide, S. A. Saldanha, D. Minond, T. P. Spicer, J. R. Fotsing, M. Spaargaren, J.-M. Frère, C. Bebrone, K. B. Sharpless, P. S. Hodder and V. V. Fokin, *ACS Med. Chem. Lett.*, 2010, **1**, 150–154.
- 10 R. Gup, O. Erer and N. Dilek, *J. Mol. Struct.*, 2017, **1129**, 142–151.
- 11 P. Minetti, M. O. Tinti, P. Carminati, M. Castorina, M. A. Di Cesare, S. Di Serio, G. Gallo, O. Ghirardi, F. Giorgi, L. Giorgi, G. Piersanti, F. Bartocchini and G. Tarzia, *J. Med. Chem.*, 2005, **48**, 6887–6896.
- 12 T. Harit, R. Bellaouchi, Y. Rokni, A. Riahi, F. Malek and A. Asehraou, *Chem. Biodivers.*, 2017, **14**, e1700351.
- 13 C. Proulx and W. D. Lubell, *J. Org. Chem.*, 2010, **75**, 5385–5387.
- 14 N. Das Adhikary and P. Chattopadhyay, *J. Org. Chem.*, 2012, **77**, 5399–5405.
- 15 J. R. Donald and S. F. Martin, *Org. Lett.*, 2011, **13**, 852–855.
- 16 J. Zhang and C.-W. T. Chang, *J. Org. Chem.*, 2009, **74**, 4414–4417.
- 17 S. Beghdadi, I. Abdelhedi Miladi, H. Ben Romdhane, J. Bernard and E. Drockenmuller, *Biomacromolecules*, 2012, **13**, 4138–4145.
- 18 M. J. Leonardi, M. R. Topka and P. H. Dinolfo, *Inorg. Chem.*, 2012, **51**, 13114–13122.
- 19 G. S. Huff, W. K. C. Lo, R. Horvath, J. O. Turner, X.-Z. Sun, G. R. Weal, H. J. Davidson, A. D. W. Kennedy, C. J. McAdam, J. D. Crowley, M. W. George and K. C. Gordon, *Inorg. Chem.*, 2016, **55**, 12238–12253.
- 20 T. U. Connell, J. M. White, T. A. Smith and P. S. Donnelly, *Inorg. Chem.*, 2016, **55**, 2776–2790.
- 21 W. K. C. Lo, G. S. Huff, J. R. Cubanski, A. D. W. Kennedy, C. J. McAdam, D. A. McMorran, K. C. Gordon and J. D. Crowley, *Inorg. Chem.*, 2015, **54**, 1572–1587.
- 22 J. Winn, A. Pinczewska and S. M. Goldup, *J. Am. Chem. Soc.*, 2013, **135**, 13318–13321.
- 23 E. M. Schuster, G. Nisnevich, M. Botoshansky and M. Gandelman, *Organometallics*, 2009, **28**, 5025–5031.
- 24 J. D. Crowley and D. A. McMorran, in *Click Triazoles*, ed. J. Košmrlj, Springer Berlin Heidelberg, Berlin, Heidelberg, 2012, pp. 31–83.
- 25 P. I. P. Elliott, in *Organometallic Chemistry*, eds. I. J. S. Fairlamb and J. M. Lynam, Royal Society of Chemistry, Cambridge, 2014, vol. 39, pp. 1–25.
- 26 C. M. Álvarez, L. A. García-Escudero, R. García-Rodríguez and D. Miguel, *Chem. Commun.*, 2012, **48**, 7209–7211.
- 27 C. Nolte, P. Mayer and B. F. Straub, *Angew. Chem. Int. Ed.*, 2007, **46**, 2101–2103.
- 28 S. Liu, P. Müller, M. K. Takase and T. M. Swager, *Inorg. Chem.*, 2011, **50**, 7598–7609.
- 29 D. V. Partyka, J. B. Updegraff, M. Zeller, A. D. Hunter and T. G. Gray, *Organometallics*, 2007, **26**, 183–186.
- 30 D. V. Partyka, L. Gao, T. S. Teets, J. B. Updegraff, N. Deligonul and T. G. Gray, *Organometallics*, 2009, **28**, 6171–6182.
- 31 J. E. Heckler, B. L. Anderson and T. G. Gray, *J. Organomet. Chem.*, 2016, **818**, 68–71.
- 32 Y.-C. Li, C. Qi, S.-H. Li, H.-J. Zhang, C.-H. Sun, Y.-Z. Yu and S.-P. Pang, *J. Am. Chem. Soc.*, 2010, **132**, 12172–12173.
- 33 J. Huo, H. Hu, M. Zhang, X. Hu, M. Chen, D. Chen, J. Liu, G. Xiao, Y. Wang and Z. Wen, *RSC Adv.*, 2017, **7**, 2281–2287.
- 34 J. Engel-Andreasen, I. Wellhöfer, K. Wich and C. A. Olsen, *J. Org. Chem.*, 2017, **82**, 11613–11619.
- 35 S. I. Aziz, H. F. Anwar, M. H. Elnagdi and D. H. Fleita, *J. Heterocycl. Chem.*, 2007, **44**, 725–729.
- 36 J. Kalisiak, K. B. Sharpless and V. V. Fokin, *Org. Lett.*, 2008, **10**, 3171–3174.
- 37 Y. Liu, W. Yan, Y. Chen, J. L. Petersen and X. Shi, *Org. Lett.*, 2008, **10**, 5389–5392.
- 38 X. Wang, L. Zhang, D. Krishnamurthy, C. H. Senanayake and P. Wipf, *Org. Lett.*, 2010, **12**, 4632–4635.
- 39 R. Cai, W. Yan, M. G. Bologna, K. de Silva, Z. Ma, H. O. Finklea, J. L. Petersen, M. Li and X. Shi, *Org. Chem. Front.*, 2015, **2**, 141–144.
- 40 S. Samanta, P. Ghosh and S. Goswami, *Dalton Trans.*, 2012, **41**, 2213–2226.
- 41 R. R. Maar, A. Rabiee Kenaree, R. Zhang, Y. Tao, B. D. Katzman, V. N. Staroverov, Z. Ding and J. B. Gilroy, *Inorg. Chem.*, 2017, **56**, 12436–12447.
- 42 R. Mondol and E. Otten, *Inorg. Chem.*, 2019, **58**, 6344–6355.
- 43 S. M. Barbon, J. V. Buddingh, R. R. Maar and J. B. Gilroy, *Inorg. Chem.*, 2017, **56**, 12003–12011.
- 44 S. M. Barbon, V. N. Staroverov and J. B. Gilroy, *Angew. Chem. Int. Ed.*, 2017, **56**, 8173–8177.
- 45 R. R. Maar, R. Zhang, D. G. Stephens, Z. Ding and J. B. Gilroy, *Angew. Chem. Int. Ed.*, 2019, **58**, 1052–1056.
- 46 M.-C. Chang and E. Otten, *Inorg. Chem.*, 2015, **54**, 8656–8664.
- 47 R. Mondol, D. A. Snoeken, M.-C. Chang and E. Otten, *Chem. Commun.*, 2017, **53**, 513–516.
- 48 M.-C. Chang, T. Dann, D. P. Day, M. Lutz, G. G. Wildgoose and E. Otten, *Angew. Chem. Int. Ed.*, 2014, **53**, 4118–4122.
- 49 R. Travieso-Puente, J. O. P. Broekman, M.-C. Chang, S. Demeshko, F. Meyer and E. Otten, *J. Am. Chem. Soc.*, 2016, **138**, 5503–5506.
- 50 S. Hong, L. M. R. Hill, A. K. Gupta, B. D. Naab, J. B. Gilroy, R. G. Hicks, C. J. Cramer and W. B. Tolman, *Inorg. Chem.*, 2009, **48**, 4514–4523.
- 51 D. L. J. Broere, B. Q. Mercado, J. T. Lukens, A. C. Vilbert, G. Banerjee, H. M. C. Lant, S. H. Lee, E. Bill, S. Sproules, K. M. Lancaster and P. L. Holland, *Chem. – Eur. J.*, 2018, **24**, 9417–9425.
- 52 F. Milocco, S. Demeshko, F. Meyer and E. Otten, *Dalton Trans.*, 2018, **47**, 8817–8823.

- 53 E. Kabir, C.-H. Wu, J. I.-C. Wu and T. S. Teets, *Inorg. Chem.*, 2016, **55**, 956–963.
- 54 E. Kabir, D. Patel, K. Clark and T. S. Teets, *Inorg. Chem.*, 2018, **57**, 10906–10917.
- 55 E. Kabir, G. Mu, D. A. Momtaz, N. A. Bryce and T. S. Teets, *Inorg. Chem.*, 2019, **58**, 11672–11683.
- 56 R. Mondol and E. Otten, *Inorg. Chem.*, 2018, **57**, 9720–9727.
- 57 G. Mu, L. Cong, Z. Wen, J. I.-C. Wu, K. M. Kadish and T. S. Teets, *Inorg. Chem.*, 2018, **57**, 9468–9477.
- 58 R. Travieso-Puente, S. Budzak, J. Chen, P. Stacko, J. T. B. H. Jastrzebski, D. Jacquemin and E. Otten, *J. Am. Chem. Soc.*, 2017, **139**, 3328–3331.
- 59 H. Na and T. S. Teets, *J. Am. Chem. Soc.*, 2018, **140**, 6353–6360.
- 60 H. Na, A. Maity, R. Morshed and T. S. Teets, *Organometallics*, 2017, **36**, 2965–2972.
- 61 J.-H. Shon and T. S. Teets, *Inorg. Chem.*, 2017, **56**, 15295–15303.
- 62 P. Lai and T. S. Teets, *Chem. – Eur. J.*, 2019, **25**, 6026–6037.
- 63 J. Li, P. I. Djurovich, B. D. Alleyne, M. Yousufuddin, N. N. Ho, J. C. Thomas, J. C. Peters, R. Bau and M. E. Thompson, *Inorg. Chem.*, 2005, **44**, 1713–1727.
- 64 J. B. Gilroy, P. O. Otieno, M. J. Ferguson, R. McDonald and R. G. Hicks, *Inorg. Chem.*, 2008, **47**, 1279–1286.
- 65 M. Nonoyama, *Bull. Chem. Soc. Jpn.*, 1974, **47**, 767–768.
- 66 T. Peng, Y. Yang, Y. Liu, D. Ma, Z. Hou and Y. Wang, *Chem. Commun.*, 2011, **47**, 3150–3152.
- 67 G. M. Sheldrick, *Acta Crystallogr. A*, 2008, **64**, 112–122.



Sterically encumbered iridium-bound formazanate ligands undergo redox-neutral cyclization to form azo-triazolides, a new class of redox-active chelating ligand.